Broadening and intensity redistribution in the Na($3p$) hyperfine excitation spectra due to optical pumping in the weak excitation limit

I. Sydoryk, N. N. Bezuglov,* I. I. Beterov,† K. Miculis, E. Saks, A. Janovs, P. Spels, and A. Ekers
Laser Centre, University of Latvia, LV-1002 Riga, Latvia
(Received 6 February 2008; published 30 April 2008)

Detailed analysis of spectral line broadening and variations in relative intensities of hyperfine spectral components due to optical pumping is presented. Hyperfine levels of sodium $3p_{1/2}$ and $3p_{3/2}$ levels are selectively excited in a supersonic beam at various laser intensities under the conditions when optical pumping time is shorter than transit time of atoms through the laser beam. The excitation spectra exhibit significant line broadening at laser intensities well below the saturation intensity, and redistribution of intensities of hyperfine spectral components is observed, which in some cases is contradicting with intuitive expectations. Theoretical analysis of the dynamics of optical pumping shows that spectral line broadening sensitively depends on the branching coefficient of the laser-driven transition. Analytical expressions for branching ratio dependent critical Rabi frequency and critical laser intensity are derived, which give the threshold for onset of noticeable line broadening by optical pumping. The critical laser intensity has its smallest value for transitions with branching coefficient equal to 0.5, and it can be much smaller than the saturation intensity. Transitions with larger and smaller branching coefficients are relatively less affected. The theoretical excitation spectra were calculated numerically by solving density matrix equations of motion using the split propagation technique, and they well-reproduce the observed effects of line broadening and peak intensity variations. The calculations also show that presence of dark (i.e., not laser coupled) Zeeman sublevels in the lower state results in effective branching coefficients which vary with laser intensity and differ from those implied by the sum rules, and this can lead to peculiar changes in peak ratios of hyperfine components of the spectra.

DOI: 10.1103/PhysRevA.77.042511 PACS number(s): 32.70.Jz, 32.80.Xx

I. INTRODUCTION

Optical pumping is the well-known phenomenon that is usually associated with redistribution of population within hyperfine (HF) components or Zeeman sublevels of the ground state due to coupling by resonant light fields [1]. Optical pumping is being exploited in various applications, like cooling below the Doppler limit [2,3], vibrational excitation of molecules in the electronic ground state [4], orientation and alignment of atomic and molecular ground states [5], etc. When optical pumping is involved in the control of quantum states it is usually associated with large laser intensities exceeding the saturation limit [3]. Therefore the populations of quantum states depend nonlinearly on laser intensities and the excitation spectra are affected by power broadening [6].

In the present study we are concerned with line-shape effects due to optical pumping in the weak excitation limit. Specifically, we measure laser excitation spectra of the $3p_{1/2}$ and $3p_{3/2}$ states of Na in a supersonic beam. Coupling of the $F''=1$ and $F''=2$ levels of the ground state with different HF components of the upper states allows us to study two-level systems with different branching coefficients. The smaller the branching coefficient, the more population irreversibly leaves the two-level system, and vice versa. At very low laser intensities the excitation spectra do not reveal any abnormalities. When laser intensity is increased but still below the saturation intensity, essential modification of the excitation spectra is observed: most of the hyperfine spectral components exhibit additional broadening while their intensity ratios cease to obey the line strengths rules. Note that usually line broadening is considered to be a strong-field effect due to power broadening at laser intensities above the saturation intensity [3,6].

Since the experiments were performed at low number densities of sodium atoms ($n_{3s}\sim 10^{10}$ cm^{-3}), line-shape modifications by radiation trapping can be disregarded [7,8]. We attribute the observed line-shape effects to optical pumping, which leads to depletion broadening of spectral lines [9,10]. If transit time τ_{tr} of atoms through the laser beam is much larger than lifetime τ_{nat} of the $3p$ state, populations of levels and the associated fluorescence signals can become nonlinear on laser intensity I_{las} long before the saturation limit is reached (i.e., at $I_{las}\ll I_{sat}$). Due to interaction with laser field the ground state g has a finite width [2,11]

$$\Gamma'' = \Omega^2 \frac{\Gamma_{nat}}{\Gamma_{nat}^2 + 4\delta^2}, \tag{1}$$

where $\Gamma_{nat}=2\pi\Delta\nu_{nat}=1/\tau_{nat}$ is the natural width (in units of angular frequency [s^{-1}]) of the excited state e, δ is the laser detuning from the line center, and Ω is the Rabi frequency of the transition. The width Γ'' is equal to the rate of photons spontaneously emitted from state e. If the level system is partially open, only the fraction Π of the spontaneous transitions will return the population to the initial state g; the fraction $1-\Pi$ associated with decay to levels other than g will be lost from the (g,e)-system during each excitation-

*Also at: Fock Institute of Physics, St. Petersburg State University, 198904 St. Petersburg, Russia.

†Permanent address: Institute of Semiconductor Physics SB RAS, 630090, Novosibirsk, Russia.

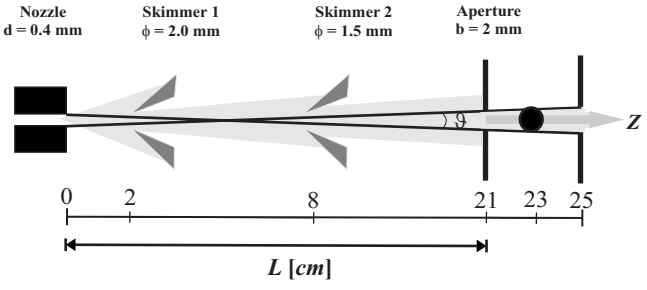

FIG. 1. Collimation of the sodium beam by skimmers and apertures. The laser beam crosses the atomic beam at right angles 23 cm downstream from the nozzle.

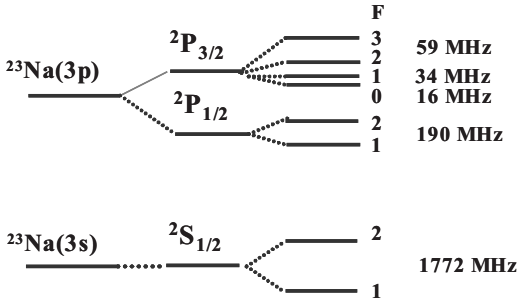

FIG. 2. Hyperfine energy levels of the $3s$ and $3p$ states of Na.

emission cycle. The rate of such pumping is obviously $\Gamma_{pump}=(1-\Pi)\Gamma''$. Hence the pumping time can be written as

$$\tau_{pump}(\delta)=\frac{1}{\Gamma_{pump}}=\frac{\Gamma_{nat}^2+4\delta^2}{\Gamma_{nat}\Omega^2(1-\Pi)}. \quad (2)$$

If the transit time τ_{tr} is long, such that $\tau_{tr}>\tau_{pump}^{(0)}\equiv\tau_{pump}(\delta=0)$, the population of the (g,e)-system will be fully depleted during interaction with the laser field. In terms of Rabi frequencies the condition for population depletion can be rewritten as $\Omega>\Omega_{cr}\cong\Omega_{sat}\sqrt{2\tau_{nat}/[\tau_{tr}(1-\Pi)]}$, where the saturation Rabi frequency is $\Omega_{sat}=\Gamma_{nat}/\sqrt{2}$ [3]. Note that the parameter $1/\sqrt{\tau_{nat}\tau_{tr}}$, which was considered in [5,12] as the parameter associated with saturation due to optical pumping in the case of open level systems (i.e., no population return from state e to state g), is identical to our critical Rabi frequency Ω_{cr} in the limiting case of $\Pi=0$.

If the weak excitation limit is combined with long interaction times of atoms with the laser field, such that $\tau_{tr}\gg\tau_{nat}$, the value of critical Rabi frequency is small ($\Omega_{cr}<\Omega_{sat}$) and broadening and saturation of spectral lines can be observed at laser intensities well below the saturation limit, long before power broadening starts affecting the line shapes.

II. EXPERIMENT

The experiment was performed in a supersonic beam of Na atoms (see Fig. 1). Two skimmers and an entrance aperture of the excitation zone collimate the beam with flow velocity v_f to a small divergence angle ϑ, thus reducing the Doppler width for excitation perpendicular to the beam axis to $\Delta\nu_D\equiv v_f\vartheta/(2\lambda)$, where λ is the laser wavelength. The divergence angle ϑ was set to either 0.67° or 0.92° by using the entrance aperture b of either 2 or 3 mm diameter. The laser beam crosses the atomic beam at right angles, and it is linearly polarized parallel to the molecular beam axis z, which is also the quantization axis. Only Zeeman sublevels with identical quantum numbers m_F are coupled by the laser field due to the selection rule $\Delta m_F=0$, while for transitions between levels with the same F the transition $m_{F''}=0\leftrightarrow m_{F'}=0$ is forbidden. The number density of atoms in the beam was chosen sufficiently low ($\leq 10^{10}$ cm^{-3}), thus ensuring that the beam is not optically thick and effects of radiation trapping and photon reabsorption [8] can be safely neglected.

An important consequence of optical transparency of the beam is that absorption $P(\Delta\nu_L)$ (the total number of photons absorbed per second) and excitation $J(\Delta\nu_L)$ (the integrated over frequencies flux of emitted photons in the direction of observation) profiles as a function of the laser detuning $\Delta\nu_L$ do not vary in the interaction volume defined by the crossing atomic and laser beams. Both profiles are proportional to the integral (over the interaction volume and HF sublevels) population of the excited state.

The $3s\rightarrow 3p$ transition was excited using a single mode cw radiation source (Coherent CR-699–21 dye laser) with a linewidth of 1 MHz. The fluorescence emitted by Na atoms was collected into two fiber bundles at the angles of 90° and 45° with respect to the directions of the axis of the molecular beam, laser beam, and laser polarization. The fluorescence light was guided via the fiber bundles to two photomultipliers, and the signals proportional to $J(\Delta\nu_L)$ were registered using photon counters. The resulting excitation spectra of the $3p$ state were recorded as a function of laser detuning $\Delta\nu_L$. The arrangement with two different simultaneous detection geometries allowed us to verify that radiation trapping, which is strongly anisotropic with respect to the direction of the observation, does not affect the measured spectra. It also allowed us to rule out the influence of polarization effects on variations in line shapes and relative line intensities.

The mean flow velocity v_f of atoms in the beam was measured to be 1160 m/s. For excitation perpendicular to the atomic beam axis the apertures of the excitation zone of $b=2$ and 3 mm correspond to the residual Doppler width $\Delta\nu_D=11.2$ and 15.9 MHz [full width at half maximum (FWHM)], respectively. These should be compared to the excitation perpendicular to the natural width of $\Delta\nu_{nat}$ of 9.8 MHz ($\tau_{nat}=16.23$ ns for the $3p_{3/2}$ [13]).

Figure 2 shows the hyperfine energy levels of the $3s$ and $3p$ states. The excitation spectra were obtained by scanning the laser frequency across the $3s_{1/2}\rightarrow 3p_{1/2}$ and $3s_{1/2}\rightarrow 3p_{3/2}$ transitions. The HF splittings are larger than both the Doppler width and the natural width for all but one pair of components ($3p_{3/2}$ $F'=0$ and $F'=1$). The measurements for the D_1 line ($\lambda=589.593$ nm) were performed with the aperture $b=2$ mm. In the case of the D_2 line ($\lambda=588.996$ nm), $b=3$ mm was used. The radius of the laser beam was $r_{las}=1.5$ mm, which corresponds to the transit time $\tau_{tr}=2r_{las}/v_f=2.65$ μs at $v_f=1160$ m/s. Thus the transit time is by more than two orders of magnitude larger than the natural lifetime of the $3p$ state.

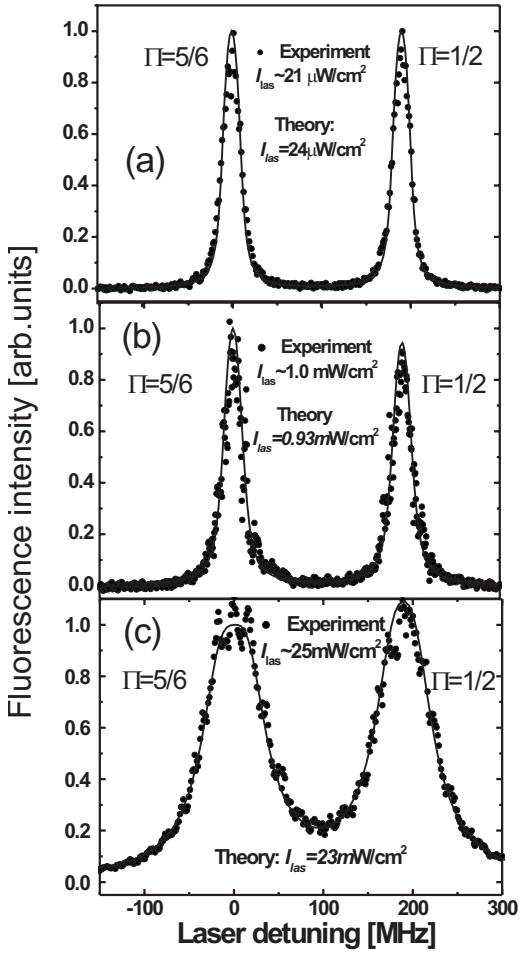

FIG. 3. Excitation spectra of the $3s_{1/2}$, $F''=2\rightarrow 3p_{1/2}$, $F'=1,2$ transitions in Na. Residual Doppler width due to finite collimation angle is $\Delta\nu_D=11.2$ MHz (at $b=2$ mm). The expected peak ratio is 1:1. Saturation intensities of the lhs and rhs components are 7.5 and 12.5 mW/cm^2, respectively.

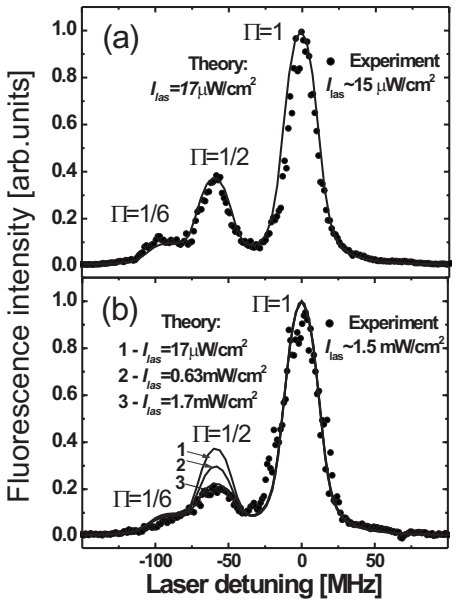

FIG. 4. Excitation spectra of the $3s_{1/2}$, $F''=2\rightarrow 3p_{3/2}$, $F'=1,2,3$ transitions in Na. Residual Doppler width due to finite collimation angle is $\Delta\nu_D=15.9$ MHz (at $b=3$ mm). The expected peak ratio is 1:5:14. Saturation intensities of the three components are 37.4, 12.5, and 6.2 mW/cm^2, respectively.

III. SPECTRA

Figure 3 shows the measured excitation spectra of the $3p_{1/2}$ state from the $F''=2$ sublevel of the ground state at various laser intensities. The spectra exhibit two peaks corresponding to the excitation of the $3s_{1/2}$, $F''=2\rightarrow 3p_{1/2}$, $F'=1,2$ HF transitions. The spectra of Fig. 3 were measured at the divergence angle of the atomic beam of $\vartheta=0.67°$, which corresponds to residual Doppler width of $\Delta\nu_D=11.2$ MHz (see Sec. VI for details on Doppler line shape). The spectrum of Fig. 3(a) was measured at a very low laser intensity of 21 μW/cm^2. Both HF components appear equally strong, which is obviously due to equal line strengths of both HF transitions [14]. The line shapes are determined by a combined effect of natural ($\Delta\nu_{nat}=9.8$ MHz) and Doppler broadening. In Fig. 3(b) the laser intensity has been increased by a factor of about 70 compared to Fig. 3(a) to the value of 1 mW/cm^2, which is still much smaller than the saturation intensity of both HF components (7.5 and 12.5 mW/cm^2). One can observe that the $F''=2\rightarrow F'=2$ [right-hand side (rhs)] component has become somewhat smaller than the $F''=2\rightarrow F'=1$ [left-hand side (lhs)] component. Peculiarly, when the laser intensity is further increased to 25 mW/cm^2 [Fig. 3(c)], the rhs component becomes somewhat larger than the lhs component, while the widths of the peaks ($\Delta\nu=75$ MHz) are substantially larger than the width $\Delta\nu_{sat}=16.5$ MHz expected from saturation broadening at this laser intensity.

The $3s_{1/2}$, $F''=2\rightarrow 3p_{3/2}$, $F'=1,2,3$ excitation spectra are shown in Fig. 4. The relative peak intensities match the theoretical line strengths of individual HF transitions when laser intensity is very small [15 μW/cm^2, Fig. 4(a)]. When laser intensity is increased to 1.5 mW/cm^2, which is still below the saturation intensity, the relative intensities of the components corresponding to the excitation of the $F'=1$ and $F'=2$ HF levels are smaller than expected from the theoretical line strengths [Fig. 4(b)]. When laser intensity is close to saturation intensity, the $F'=1$ and $F'=2$ peaks are so weak compared to the $F'=3$ peak that it is ambiguous to attempt analysis of their linewidth.

The $3s_{1/2}$, $F''=1\rightarrow 3p_{1/2}$, $F'=1,2$ excitation spectra are shown in Fig. 5. Like in the case of Fig. 3, also here a significant broadening is observed at laser intensities below the saturation limit. In contrast to Fig. 3(b), however, the lhs peak corresponding to the excitation of the $F'=1$ component of the upper state grows monotonically as compared to the rhs peak.

IV. THEORETICAL LINE STRENGTHS AND SATURATION INTENSITY

At very small laser intensities the strengths of individual peaks in the excitation spectra shown in Figs. 3–5 correspond to the respective theoretical line strengths $S_i^{(j)}$ of individual HF transitions $i=\{F''\rightarrow F'\}$ within the D_1 ($j=1/2$) or

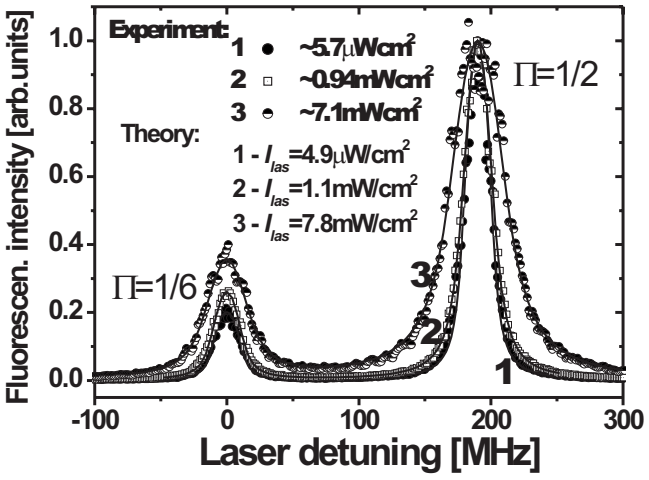

FIG. 5. Excitation spectra of the $3s_{1/2}$, $F''=1\rightarrow 3p_{1/2}$, $F'=1,2$ transitions in Na. Residual Doppler width due to finite collimation angle is $\Delta\nu_D=11.2$ MHz (at $b=2$ mm). The expected peak ratio is 1:5. Saturation intensities of the lhs and rhs components are 37.4 and 12.5 $\mathrm{mW/cm^2}$, respectively.

D_2 ($j=3/2$) lines [14]. The values of $S_i^{(j)}$ are directly related to the reduced matrix elements of the transitions and the partial natural width of the respective transition:

$$S_i^{(j)} = |(1/2,F''\|D\|j,F')|^2;$$

$$\Gamma_{nat}^{(i)} = \frac{4\omega_i^3}{3\hbar c^3}\frac{1}{2F'+1}S_i^{(j)}. \tag{3}$$

Intensity of the component i is proportional to its line strength because the product $\Gamma_{nat}^{(i)}(2F'+1)$ regulates the photon flux of this component under the conditions of thermodynamic equilibrium [14]. Figure 6 shows the theoretical line strengths $\tilde{S}_i^{(j)}$ (square frames) in units of the reduced matrix element $|(3s\|D\|3p)|^2$ of the unresolved $3s\rightarrow 3p$ transition, i.e., $S_i^{(j)}=\tilde{S}_i^{(j)}|(3s\|D\|3p)|^2$. The values of $\tilde{S}_i^{(j)}$ are normalized such that $\Sigma_{j,i}\tilde{S}_i^{(j)}=8$ [14]. Thus the theoretical values of peak ratios can be directly taken from Fig. 6, and they agree with

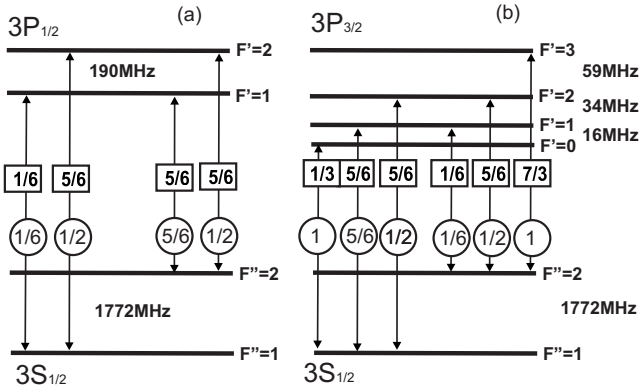

FIG. 6. Line strengths $\tilde{S}_i^{(j)}$ (square frames) and branching ratios Π_i (circular frames) for (a) $3s_{1/2}\rightarrow 3p_{1/2}$ and (b) $3s_{1/2}\rightarrow 3p_{3/2}$ hyperfine transitions.

the experimental observations at very small laser intensities [see Figs. 3(a) and 4(a)].

Saturation intensity of each hyperfine transition depends on the natural width of the transition $\Delta\nu_{nat}$ and the branching ratio Π_i [3] (see also in Sec. V):

$$I_{sat}^{(i)} = \frac{4\pi^3\hbar c}{3\lambda_i^3}\frac{\Delta\nu_{nat}}{\Pi_i}. \tag{4}$$

The values of the hyperfine branching coefficients Π_i (circular frames in Fig. 6) are easily obtained from the reduced line strengths $\tilde{S}_i^{(j)}$. Note that all HF transitions have the same natural width of $\Delta\nu_{nat}=9.8$ MHz.

The saturation intensity given by Eq. (4) gives the limiting laser intensity after which stimulated transitions start transforming the excitation spectra [3]. The lowest laser intensities used in measurements of the spectra shown in Figs. 3–5 are much smaller than saturation intensity $I_{sat}^{(i)}$ of any of the HF transitions. Therefore one naturally expects the peak ratios to be in accordance with the line strengths of Fig. 6 and the linewidth to correspond to the residual Doppler width determined by beam divergence. This agrees with the observations made for the smallest laser intensities.

When laser intensity is increased by a factor of about 100, it is still well below the saturation intensity $I_{sat}^{(i)}$. Nevertheless, a curious transformation of the spectra is observed: widths of the peaks increase, and peak ratios of the HF components change. Interestingly, the strongest $F''=2\rightarrow F'=3$ component of the D_2 line (Fig. 4) is not affected by broadening at all although its saturation intensity $I_{sat}^{(i)}=6.2$ $\mathrm{mW/cm^2}$ is the smallest. Intuitively, one would expect the transition $F''=2\rightarrow F'=3$ to be the first one that is affected by broadening when laser intensity is increased.

Not only the widths are affected. Relative intensities of the HF peaks change as laser intensity is increased. At first glance it seems that relative intensities of components with smaller branching ratios Π_i should decrease when optical pumping becomes non-negligible, as less population returns to the lower laser coupled level than it does for levels with larger Π_i. This is clearly the case in Figs. 3(b), but not in the case of Fig. 5. Moreover, Fig. 3 shows another unexpected feature: after the intensity of the peak with smaller Π_i has initially decreased with respect to the peak with larger Π_i [cf., Figs. 3(a) and 3(b)], a further increase of laser intensity leads to an increase of the peak with smaller Π_i [cf., Figs. 3(b) and 3(c)]. Explanation of these observations requires a detailed analysis of the dynamics of optical pumping.

V. DYNAMICS OF OPTICAL PUMPING AND ITS EFFECT ON THE FLUORESCENCE SIGNALS

The measured fluorescence signals are affected by various factors like the detection efficiency and geometry. The spectral components are excited and detected at very close wavelengths under identical conditions, therefore it can be safely assumed that the detection efficiency is equal for all of them. Since we are interested in relative intensities and widths of the components, it is sufficient to consider the fluorescence signals that are proportional to the total number of photons

emitted by atoms at all times in all directions.

We consider the following model problem. Two-level atoms with the ground state g and the excited state e propagate along the z axis with the flow velocity of the beam v_f. The atoms cross the laser beam with radius r_{las}, frequency ω, and Gaussian intensity distribution

$$I(z) = I_{las} \exp(-z^2/r_{las}^2);$$

$$\tau_{tr} = 2r_{las}/v_f. \tag{5}$$

Such distribution corresponds to Gaussian switching of Rabi frequency Ω of the g-e transition:

$$\Omega(t) = \Omega_0 \exp(-2t^2/\tau_{tr}^2);$$

$$t = z/v_f. \tag{6}$$

The value $\Omega_0 = E_0\langle g|d_z|e\rangle$ is the Rabi frequency of the g-e coupling in the center of the laser beam which is linearly polarized parallel to the z axis.

A. Evaluation of the fluorescence signal

In what follows we shall assume that the transit time is much larger than the lifetime of the upper state, $\tau_{tr} \gg \tau_{nat}$, which is true for the parameters of our experiment. This allows us to use the adiabatic elimination for the nondiagonal density matrix element ρ_{eg} [15]:

$$\rho_{eg}(t) = \frac{i\Omega(t)}{\Gamma_e - i2\delta}[n_g(t) - n_e(t)]. \tag{7}$$

The above equation relates $\rho_{eg}(t)$ to the populations $n_g(t) = \rho_{gg}(t)$ and $n_e(t) = \rho_{ee}(t)$. The decay rate $\Gamma_e = 1/\tau_{nat}$ gives the natural width of the level e, while $\delta = 2\pi\Delta\nu_L$ is the laser detuning. With ρ_{eg} defined by Eq. (7), the time evolution of the populations is given by simple balance equations:

$$\frac{d}{dt}n_e = -\Gamma_e n_e + r(t)(n_g - n_e); \tag{8}$$

$$\frac{d}{dt}n_g = \Pi\Gamma_e n_e + r(t)(n_e - n_g). \tag{9}$$

The first equation describes the population loss from level e via two processes: (i) spontaneous decay at the rate Γ_e, and (ii) stimulated emission at the rate equal to the optical pumping rate $r(t)$:

$$r(t) = \Gamma_e \frac{\Omega^2(t)}{4\delta^2 + \Gamma_e^2}. \tag{10}$$

The population of level g is affected by three competing processes: (i) photon absorption at the rate $r(t)$ resulting in the population of level e, (ii) return of population from level e to level g due to stimulated emission, and (iii) return of population from level e to level g due to spontaneous emission. The rate of the latter is determined by the branching coefficient Π of the given HF transition. The branching coefficients are normalized such that $\Pi = 0$ for an entirely open system (no spontaneous return from level e to level g) and $\Pi = 1$ for a closed system (no transitions outside the g-e system).

The initial conditions of Eqs. (8) and (9) follow from the requirement that initially all the population is in level g while level e is not populated: $n_g(t=-\infty) = 1$; $n_e(t=-\infty) = 0$. The assumption $\tau_{tr} > \tau_{nat}$ leads to a further simplification of Eqs. (8) and (9) in the weak excitation limit, when $r(t) < 0.5\Gamma_e$. As weak excitation we understand excitation at laser intensities smaller than the saturation intensity given by Eq. (4), i.e., when Rabi frequency of the transition does not exceed the saturated value, $\Omega_0 < \Omega_{sat}$, where $\Omega_{sat} \equiv \Gamma_e/\sqrt{2}$ [3]. In that case, the adiabatic elimination implies that $dn_e/dt = 0$ [15], and Eq. (8) immediately yields

$$-\Gamma_e n_e + r(t)(n_g - n_e) = 0 \Rightarrow n_e(t) = \frac{r(t)}{\Gamma_e}[n_g(t) - n_e(t)]. \tag{11}$$

Equation (9) can then be transformed into the form

$$\frac{d}{dt}\left[\left(1 + \frac{r}{\Gamma_e}\right)n_-\right] = -r(t)(1-\Pi)n_-(t);$$

$$n_-(t) \equiv n_g(t) - n_e(t). \tag{12}$$

The above equation can be comfortably used for the evaluation of the fluorescence signal J. Integration of both sides of Eq. (8) yields the total number of spontaneous photons emitted by the excited atoms:

$$J = \Gamma_e \int_{-\infty}^{\infty} dt\, n_e(t) = \int_{-\infty}^{\infty} dt\, r(t) n_-. \tag{13}$$

Integration of Eq. (12) and combination of the result with Eq. (13) yields

$$(1-\Pi)J = 1 - n_-(t=\infty) = 1 - n_g(t=\infty). \tag{14}$$

The above expression has a straightforward physical meaning: the number of spontaneously emitted photons on transitions outside the g-e system is equal to the total loss of ground state population during interaction with the laser field.

Using Eqs. (12) and (14), we can derive the fluorescence signal in an explicit analytical form:

$$J = \frac{1}{(1-\Pi)}\{1 - \exp[-(1-\Pi)R]\};$$

$$R = \int_{-\infty}^{\infty} dt \frac{r(t)}{1 + r(t)/\Gamma_e}. \tag{15}$$

Since we consider the case of weak excitation when $r(t) < 0.5\Gamma_e$, the integral R in Eq. (15) further simplifies to the form

$$R \cong \int_{-\infty}^{\infty} dt r(t) = \frac{\sqrt{\pi}\Gamma_e \tau_{tr}}{2} \frac{\Omega_0^2}{4\delta^2 + \Gamma_e^2};$$

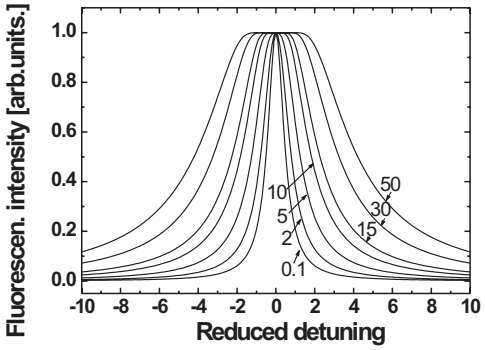

FIG. 7. Signal J [Eq. (17)] as a function of the reduced detuning δ/Γ_e for different values of the pumping parameter P_{pump} (shown as labels of the curves).

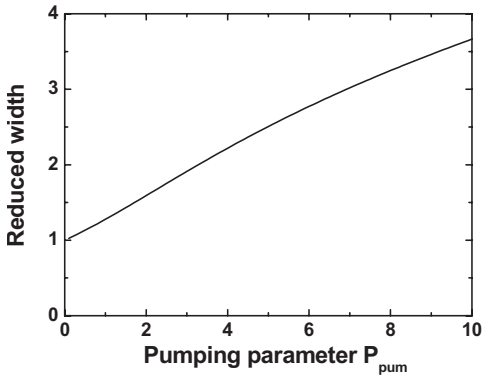

FIG. 8. The reduced width $\Delta\nu_{pum}/\Delta\nu_{nat}$ given by Eq. (19) as a function of the pumping parameter P_{pump}.

$$\Omega_0 < \Omega_{sat} \equiv \Gamma_e/\sqrt{2}. \tag{16}$$

Dependence of the fluorescence signal on the laser detuning $\delta=2\pi\Delta\nu_L$ can now be rewritten as

$$J(\delta) = \frac{\sqrt{\pi}\Omega_0^2\tau_{tr}}{2\Gamma_e}\frac{1}{P_{pump}}\left[1-\exp\left(-\frac{P_{pump}}{1+4(\delta/\Gamma_e)^2}\right)\right];$$

$$P_{pump} = \frac{\tau_{tr}}{\tau_{pump}^{(0)}};$$

$$\tau_{pump}^{(0)} = \frac{2\Gamma_e}{\sqrt{\pi}\Omega_0^2(1-\Pi)}. \tag{17}$$

The above equation shows that the excitation spectrum strongly depends on the pumping parameter P_{pump}, which is given by the ratio of transit time τ_{tr} and pumping time $\tau_{pump}^{(0)}$. The latter was already discussed in Sec. I [Eq. (2)], and it has the meaning of optical pumping time at resonant excitation ($\delta=0$). Importantly, the parameter P_{pump} can be large even at laser intensities well below the saturation limit: $P_{pump}\gg 1$ when $\tau_{tr}\gg\tau_{pum}^{(0)}$ and $\Omega_0\ll\Omega_{sat}$.

B. Line broadening by optical pumping

When the pumping parameter is small ($P_{pump}\ll 1$), Eq. (17) simplifies to yield the ordinary Lorentz line shapes:

$$J_L(\delta) = R = \frac{\sqrt{\pi}\Omega_0^2\tau_{tr}}{2\Gamma_e}\frac{1}{1+4(\delta/\Gamma_e)^2}. \tag{18}$$

When P_{pump} is increased, Eq. (18) no longer holds and Eq. (17) must be used. An almost tenfold increase of the linewidth is observed as P_{pump} is increased from 0.1 to 50 (see Fig. 7). Such broadening has a simple explanation. Consider a near resonant case, when $\Delta\nu_L=\delta/2\pi\approx 0$. Starting from values $P_{pump}\approx 1$ the atoms spend sufficient time in the laser field for the population of the ground state to be depleted, $n_g(t=\infty)\approx 0$. Depletion of level g is associated with the emission of a fixed number of photons $1/(1-\Pi)$ [see Eq. (14)]. Hence optical pumping saturates the observed signal $I(\delta\approx 0)$ via depletion saturation, provided that $\tau_{pump}(\delta) > \tau_{tr}$. Further increase of P_{pump} cannot increase the number of photons emitted upon excitation at the line center. At the same time, the number of photons emitted upon excitation in the wings continues increasing with P_{pump} until depletion saturation is reached at consecutively larger laser detunings δ. Therefore linewidths in the excitation spectra will increase with P_{pump}, and line shapes will exhibit the characteristic flat-top peaks at large P_{pump}.

The relative increase of the width $\Delta\nu_{OP}=\delta_{OP}/2\pi$ (FWHM) of the line profile affected by optical pumping as compared to the natural width can be easily obtained from Eq. (17):

$$\frac{\Delta\nu_{OP}}{\Delta\nu_{nat}} = \sqrt{\frac{P_{pump}}{\ln 2 - \ln[1+\exp(-P_{pump})]}} - 1;$$

$$\Delta\nu_{nat} = \Gamma_e/2\pi. \tag{19}$$

Variation of the width with P_{pump} is shown on Fig. 8. As can be seen, the broadening becomes noticeable at about $P_{pump}=1$, and further increase of the width scales as the square root of P_{pump} for large values of P_{pump}.

The condition $P_{pump}>1$ for broadening by optical pumping can be reformulated in terms of Rabi frequencies, i.e., Rabi frequency of the laser-driven transition must be larger than some critical value Ω_{cr}:

$$\Omega > \Omega_{cr} = \sqrt{\frac{2}{\pi^{1/2}\tau_{nat}\tau_{tr}(1-\Pi)}}; \tag{20}$$

$$\Omega_{cr} = \Omega_{sat}\sqrt{\frac{2\tau_{nat}}{\tau_{tr}(1-\Pi)}}. \tag{21}$$

Inequality (20) generalizes the results obtained in [5,12] for the limit of entirely open level systems with $\Pi=0$, which is often used as an approximation in the case of molecules with many possible rovibronic transitions. Broadening by optical pumping turns out to be sensitively dependent on the branching ratio Π. In the limit of a closed level system ($\Pi=1$) Ω_{cr} is formally equal to infinity. It is not surprising: if there are two isolated quantum states, then no pumping can occur regardless of how strong the exciting laser field is.

It is important to note that the above described broadening mechanism differs from the classical textbook examples of saturation and power broadening [6]. In [6], the saturation broadening is attributed to the strong field effects, when light-induced pumping rate becomes comparable to the relaxation rates, while the power broadening is attributed to a considerable Rabi flopping frequency. The saturation parameter in both cases is given by the ratio of pumping rate to relaxation rate. In our considered case, in contrast, the pumping rate is very small, laser intensity is well below the traditional saturation intensity given by Eq. (4), yet a notable depletion of level g is reached via optical pumping in a partially open two-level system due to long interaction time with the laser field; the line broadening thus occurs in the weak excitation limit, when $n_e(t) \ll n_g(t)$.

Line broadening by optical pumping is thus the dominating line broadening mechanism when $\Omega_{crit} < \Omega < \Omega_{sat}$. At $\Omega > \Omega_{sat}$ the rate of laser-induced transitions exceeds the spontaneous transition rate. When the splitting ($\sim\Omega$) of laser dressed states exceeds their widths, the population is equally shared between the levels e and g [2,16]. The pumping time $\tau_{pump}(0)$ then stabilizes at $2/[\Gamma_e(1-\Pi)]$ and becomes independent of further increases of laser intensity.

C. Critical laser intensity

It is useful to rewrite Eq. (20) in terms of laser intensities, since those are usually used by experimentalists. We shall therefore express the laser intensity in terms of the transition Rabi frequency as follows:

$$I_{las} = \frac{4\pi^2\hbar c}{3\lambda^3}\frac{\Omega^2}{\Gamma_e \Pi}. \tag{22}$$

The above equation is well-known for closed systems with $\Pi = 1$ [3]. In the case of a partially open system we have replaced the natural width Γ_e by the partial natural width $\Gamma_e\Pi$ of the given transition. This can be done because Rabi frequency $\Omega = Ed/\hbar$ involves the dipole element $d = \langle g|d_z|e\rangle$ associated with the partial natural broadening $\Gamma_e\Pi = 4\omega^3 d^2/3\hbar c^3$ [14]. Since $I_{las} = E^2 c/8\pi$, we obtain Eq. (22). Using Eq. (22), Eq. (20) can be rewritten as

$$I_{cr} = \frac{8\pi^2\hbar c}{\sqrt{\pi}3\lambda^3}\frac{1}{\tau_{tr}\Pi(1-\Pi)} = \frac{4\tau_{nat}}{\sqrt{\pi}\tau_{tr}(1-\Pi)}I_{sat}. \tag{23}$$

Simultaneously, the pumping parameter can now be rewritten in terms of the ratio of the actual laser intensity to the critical laser intensity:

$$P_{pum} = I_{las}/I_{cr}. \tag{24}$$

Equation (23) shows the relation between the critical laser intensity and the traditional saturation intensity [Eq. (4)], which gives the limit for onset of power broadening.

Note that formally $I_{cr} \to \infty$ when $\Pi \to 0$ (completely open system). The limit of $\Pi \to 0$ corresponds to $d \to 0$, i.e., to forbidden optical transitions. Therefore even a very small transfer of population from level g to level e will require an extremely large laser intensity.

VI. RESIDUAL DOPPLER BROADENING

Besides the broadening due to optical pumping, the spectral lines are also affected by a small but non-negligible Doppler broadening due to finite divergence angle ϑ of the atomic beam. Such divergence is associated with nonzero velocity components in the direction of the laser beam for atoms moving not exactly parallel to the atomic beam axis. For atoms experiencing the Doppler shift $\Delta\omega$ the laser detuning δ will transform into the detuning $\delta + \Delta\omega$. A corresponding replacement $\delta \to \delta + \Delta\omega$ should therefore be done in Eq. (17). The resultant profile of a line in the excitation spectrum is thus given by a sum of profiles (17) resulting from absorption of laser photons by atoms of different velocity groups. If the probability of atoms to have a velocity leading to the Doppler shift $\Delta\omega$ is $P_D(\Delta\omega)$, then the resultant line profile is given by the integral

$$J_{res}(\delta) = \int_{-\infty}^{\infty} d\Delta\omega P_D(\Delta\omega) J(\delta + \Delta\omega). \tag{25}$$

The analytical form of the function $P_D(\Delta\omega)$ for effusive beams has been derived in [17], while for the case of supersonic beams it will be analyzed in detail in [18]. This analysis builds on the following assumptions: (i) nozzle diameter d is small compared to the diameter b of the entrance aperture and distance L from the nozzle to the excitation zone (see Fig. 1); (ii) divergence angle ϑ of the atomic beam is small; (iii) size of the excitation zone $\sim r_{las}$ is small compared to the distance L, and the distribution of atoms within $\sim r_{las}$ is uniform; and (iv) the velocity distribution in the direction perpendicular to the atomic beam axis is due to the divergence of the beam with the axial velocity distribution $F(v)$. The distribution functions $F(v)$ for various kinds of beams can be found in [19].

Leaving the somewhat lengthy detailed derivation of the function $P_D(\Delta\omega)$ to the forthcoming paper [18], we shall give here the final form of the most essential core ($|\Delta\nu| < \Delta\nu_D/1.5$) part of the distribution function for the supersonic beam:

$$P_D^{(cor)}(\Delta\nu) = \frac{2}{\pi\Delta\nu_D}\sqrt{1 - \Delta\nu^2/\Delta\nu_D^2}, \tag{26}$$

with

$$\Delta\nu_D \equiv \frac{v_f}{\lambda}\frac{\vartheta}{2}; \quad \vartheta = \frac{b+d}{L}. \tag{27}$$

The values of the parameters v_f, λ, b, d, and L are given in Sec. II. Note that the function (26) deviates strongly from the Gaussian function, which is usually associated with Doppler profiles. The frequency dependence of P_D in the wings of the spectral line ($|\Delta\nu| \geq \Delta\nu_D/1.5$) differs from that given by Eq. (26). Nevertheless, in our case it is sufficient to use only the core part of P_D. Since $\Delta\nu_D$ is comparable with $\Delta\nu_{nat}$, the natural broadening outcompetes the exponentially small wings of the Doppler profile at large $\Delta\nu$ [18].

VII. RESULTS AND DISCUSSION

Calculations of the theoretical spectra are performed in two steps: (i) solution of the evolution problem for an individual atom excited by linearly polarized laser field detuned by $\Delta\nu=\delta/2\pi$, and (ii) calculation of the resultant line profile by performing the convolution (25). The first step is performed by modeling quantum dynamics of individual pairs of Zeeman sublevels m_F within the $F''m_{F''}\rightarrow F'm_{F'}$ HF transition during coupling of the levels by the electrical field of laser light distributed as $|\vec{E}|=E_0\exp(-z^2/2r_{las}^2)|\vec{e}_z\cos(\omega t)|$. Correspondingly, the spatial distribution of Rabi frequencies of individual HF transitions also follows the Gaussian distribution:

$$\Omega^{(m)}=E_0\exp(-z^2/2r_{las}^2)\langle F''m_{F''}|d_z|F'm_{F'}\rangle. \tag{28}$$

It is convenient to introduce the reduced Rabi frequency Ω_{red} associated with the unresolved $3s$-$3p$ transition:

$$\Omega_{red}\equiv\frac{E_0}{\hbar}\sqrt{|(3s\|D\|3p)|}. \tag{29}$$

Rabi frequencies of individual Zeeman components can then be calculated from Ω_{red} using the known line strengths $\tilde{S}_i^{(j)}$ given in Fig. 6 and the $6j$ symbols [14]:

$$\Omega_0^{(m)}=\Omega_{red}\sqrt{\tilde{S}_i^{(j)}}\begin{pmatrix}F'' & 1 & F'\\ -m_{F''} & 0 & m_{F'}\end{pmatrix}, \tag{30}$$

where indexes i and j indicate the chosen HF component and the chosen level of the upper state, respectively.

The values of Ω_{red} used in the calculations may be obtained from their relation to the laser intensity I_{las} [see Eq. (22)]:

$$I_{las}=\frac{4\pi^2\hbar c}{3\lambda^3}\frac{\tau_{3p}\Omega_{red}^2}{g_{3p}}, \tag{31}$$

where $g_{3p}=3$ is the statistical weight of the $3p$ state. Note that in the calculations of theoretical spectra we used Ω_{red} as the only fitting parameter. The theoretical values of I_{las} given in Figs. 3–5 were calculated from the fitted Ω_{red} values using Eq. (31), and they are in a good agreement with the experimental values calculated from measured laser power and radius of the laser beam.

For a qualitative interpretation of the experimental results it is helpful to consider a simplified model in which the populations of Zeeman components evolve independently and the resulting signal J is simply a sum of individual signals J_m with the same $m_{F''}=m_{F'}=m$: $J(\Delta\nu)=\Sigma_m J_m(\Delta\nu)$. However, in reality Zeeman sublevels are subject to spontaneous emission on transitions with $\Delta m_F=\pm 1$. As will be shown below, such cascading can significantly change the excitation spectrum as compared to the simplified treatment when couplings with $\Delta m_F=\pm 1$ are neglected.

In order to account for cascading, we have elaborated an accurate numerical algorithm allowing the integration of equations of motion for the density matrix [11,20]

$$\frac{d\rho}{dt}=-\frac{i}{\hbar}[H,\rho]-\frac{1}{2}(\Gamma\rho+\rho\Gamma)+L(\rho), \tag{32}$$

whereby Zeeman structure of all sublevels of the system depicted in Fig. 2 is taken into account. In Eq. (32), the Hamiltonian H describes the system "atom+laser field," the matrix Γ describes the spontaneous emission, and $L(\rho)$ describes the cascade effects and has a simple explicit form in the representation of polarization moments [5]. In order to achieve a fast and efficient solution of Eq. (32), we employ the split propagation technique [21,22].

A. Regular changes of line profiles

The calculated excitation spectra $J(\Delta\nu)$ in the case of very small laser intensities ($I_{las}<I_{cr}$) are shown in Figs. 3(a) and 4(a), whereby the residual Doppler broadening has been taken into account by performing the convolution (25). An excellent agreement with the experimental results is observed. One can also see that the relative peak intensities correspond to those expected from the theoretical line strengths given in Fig. 6.

The theoretical spectra in the case when $I_{cr}<I_{las}<I_{sat}$ are shown in Figs. 3(b) and 4(b). An interesting observation can be made in Fig. 3(b). Intuitively one would expect that optical pumping is manifested more strongly and at smaller laser intensities for lines with smaller values of branching ratio Π_i, when only a small fraction of population spontaneously returns to the initial level. However, this is not the case. In fact, Eq. (23) implies that the critical laser intensity I_{cr} has a minimum at $\Pi=0.5$. Therefore nonlinear effects associated with optical pumping are more pronounced for HF transitions with branching coefficients Π close to 0.5. Note that all the excited HF levels considered here have equal lifetimes (16.2 ns). Low values of $\Pi_i^{(j)}$ are thus associated with low values of both the line strengths $S_i^{(j)}$ and the individual Rabi frequencies $\Omega_0^{(m)}$, such that interaction with laser light is inefficient for transitions with small $\Pi_i^{(j)}$. Optical pumping turns out to be most pronounced for transitions with $\Pi=0.5$. This can be best seen in Fig. 5: the relative intensity of the smaller peak with $\Pi_i=1/6$ increases with respect to the stronger peak with $\Pi_i=1/2$ as the laser intensity is increased in the range $I_{cr}<I_{las}<I_{sat}$. This is because the lower level in the case of the component with $\Pi_i=1/2$ is depleted more quickly than it is in the case of the component with $\Pi_i=1/6$.

Another important consequence of optical pumping is line broadening, which can be observed when laser intensity I_{las} is close to the critical value I_{cr} [Eq. (23)] of the given transition, or when Rabi frequency Ω is close to the critical Rabi frequency Ω_{cr} given by Eq. (21). Since I_{cr} has a minimum at $\Pi=0.5$, the spectral lines with such a branching ratio are most strongly affected by broadening due to optical pumping. Dependence of the linewidth on laser intensity is illustrated in Fig. 9(a) for the $3s_{1/2}$, $F''=2\rightarrow 3p_{1/2}$, $F'=1$ transition with $\Pi_i=5/6$ (lhs peak in Fig. 3) and the $3s_{1/2}$, $F''=2\rightarrow 3p_{1/2}$, $F'=2$ transition with $\Pi_i=1/2$ (rhs peak in Fig. 3). One can see that remarkable broadening takes place at laser intensities below the saturation intensity I_{sat} [marked in Fig.

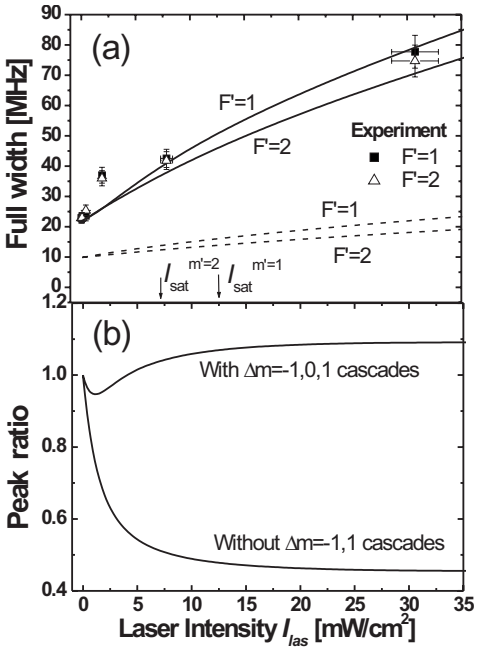

FIG. 9. (a) The FWHM widths of the lhs ($F'=1$) and rhs ($F'=2$) peaks of Fig. 3 as a function of laser intensity I_{las}. Solid squares, experiment, $F'=1$; open triangles, experiment, $F'=2$; solid curves, theory; and dashed curves, pure power broadening neglecting the broadening due to optical pumping. Arrows indicate saturation intensities of both transitions. (b) Calculated peak ratio $\Re$ of the rhs ($F'=2$) and the lhs ($F'=1$) peaks of Fig. 3 as a function of laser intensity I_{las}. The calculation was performed with and without taking the $\Delta m_F=\pm 1$ cascades into account.

9(a) with arrows], while the component with $\Pi_i=1/2$ ($F'=2$) exhibits broadening at smaller intensities than the other transition. For comparison, dashed curves in Fig. 9(a) show the intensity dependence of the power broadened linewidths calculated as $\Delta\nu_{pow}=\Delta\nu_{nat}\sqrt{1+I^2/I_{sat}^{(i)2}}$ [3]. It is immediately obvious that in the laser intensity range considered here the power broadening is much smaller than broadening due to optical pumping even at intensities exceeding the saturation intensity.

B. Irregular changes of line profiles and Zeeman structure

Variations of the excitation spectrum of the $3s_{1/2}$, $F''=2\rightarrow 3p_{1/2}$, $F'=1,2$ transitions with laser intensity (Fig. 3) are significantly different from those observed for the $3s_{1/2}$, $F''=1\rightarrow 3p_{1/2}$, $F'=1,2$ transition (Fig. 5) in two ways. (i) The relative intensity of the peak with $\Pi_i=1/2$ first decreases slightly and then increases as the laser intensity is increased. (ii) Broadening of the peak with $\Pi_i=1/2$ is actually smaller than broadening of the peak with $\Pi_i=5/6$. The key to understanding such striking differences is in the different Zeeman sublevel structures in both cases. Numerical simulations using Eq. (32), which include cascade transitions with $\Delta m_F=\pm 1$, yield a ratio $\Re$ between the peak with $\Pi_i=1/2$ and the peak with $\Pi_i=5/6$, which initially decreases with increasing laser intensity and reaches a minimum at $I_{las}\approx 1.3$ mW/cm^2 [see Fig. 9(b)]. As laser intensity is further

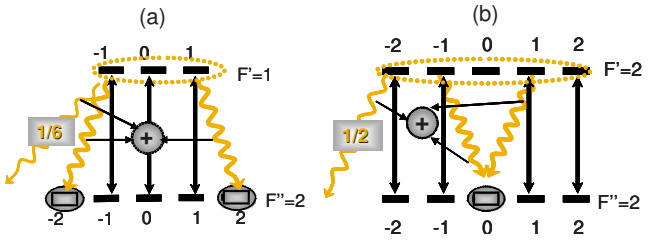

FIG. 10. (Color online) Zeeman sublevels involved in (a) the $3s_{1/2}$, $F''=2\rightarrow 3p_{1/2}$, $F'=1$ transition, and (b) the $3s_{1/2}$, $F''=2\rightarrow 3p_{1/2}$, $F'=2$ transition. Spontaneous emission leads to the population loss to the $F''=1$ level of the ground state, and to the dark $m_{F''}=\pm 2$ levels in (a) and to $m_{F''}=0$ in (b). The effective branching coefficient in case (a) is therefore $\Pi_{eff}(2,1)<5/6$ and in case (b) it is $\Pi_{eff}(2,2)<1/2$.

increased, the ratio starts growing, reaches unity at $I_{las}\approx 3.2$ mW/cm^2, and grows to values slightly larger than one. If the cascade transitions with $\Delta m_F=\pm 1$ are ignored, the calculations yield a monotonously decreasing ratio $\Re$ [lower curve in Fig. 9(a)] without any "abnormalities."

The effect of $\Delta m_F=\pm 1$ transitions becomes obvious at closer inspection of Zeeman sublevels involved in the $3s_{1/2}$, $F''=2\rightarrow 3p_{1/2}$, $F'=1$ [Fig. 10(a)] and $3s_{1/2}$, $F''=2\rightarrow 3p_{1/2}$, $F'=2$ [Fig. 10(b)] transitions. Since the laser field is linearly polarized, only the levels with the same m_F are coupled by it. The presence of "dark" levels becomes immediately obvious. In the case of the $F''=2\rightarrow F'=1$ transition, the $m_F=\pm 2$ sublevels of the lower level are not coupled by the laser field and thus act as dark states, which accumulate population channeled to them via optical pumping from the $m_F=\pm 1$ sublevels of the upper level. As a result, the branching coefficient $\Pi_i=5/6$ should be replaced by a smaller effective branching coefficient $\Pi_{eff}(F''=2,F'=1)<5/6$, which accounts for the population loss to dark states. In the case of the $F''=2\rightarrow F'=2$ transition the dark state is $m_F=0$ (due to the selection rule $\Delta m_F\neq 0$ for $F''=F'$), therefore $\Pi_{eff}(2,2)<1/2$.

Increase of laser intensity leads to a larger population of the dark states, and, consequently, to a monotonous decrease of $\Pi_{eff}(F'',F')$. At very weak laser fields $\Pi_{eff}(2,1)=5/6$, $\Pi_{eff}(2,2)=1/2$, and $I_{cr}(2,1)>I_{cr}(2,2)$ [see Eq. (23)]. Hence the transition $F''=2\rightarrow F'=2$ is more strongly affected by optical pumping than the other transition. Correspondingly, the ratio $\Re$ decreases with increasing laser intensity. As laser intensity is further increased, both $\Pi_{eff}(2,1)$ and $\Pi_{eff}(2,2)$ decrease. At some value of I_{las} both effective branching ratios satisfy the equality $\Pi_{eff}(2,1)[1-\Pi_{eff}(2,1)]=\Pi_{eff}(2,2)[1-\Pi_{eff}(2,2)]$. In that case, $I_{cr}(2,1)=I_{cr}(2,2)$, and both HF transitions are equally strongly affected by optical pumping. This corresponds to the ratio $\Re=1$ at $I_{las}=I_{eq}=3.2$ mW/cm^2 in Fig. 9(b). At $I_{las}>I_{eq}$ the value of $\Pi_{eff}(2,2)$ becomes larger than $\Pi_{eff}(2,1)$, such that $I_{cr}(2,1)<I_{cr}(2,2)$, and the ratio $\Re$ becomes larger than one. At large laser intensities the ratio $\Re$ asymptotically approaches the value of 1.09. This is because the populations of the dark $m_{F''}$ levels reach their maximum possible values when other $m_{F''}$ levels are fully depleted. In the large intensity limit the values $\Pi_{eff}(2,2)$ and $\Pi_{eff}(2,1)$ differ by only 9%, therefore both HF transitions exhibit similar broadening due to optical

pumping (see Fig. 3). In contrast, in the case of the $3s_{1/2}$, $F''=1\rightarrow 3p_{1/2}$, $F'=1,2$ transitions the component with $\Pi_i=1/2$ is apparently more strongly broadened than the component with $\Pi_i=1/6$, which could be expected (see Fig. 5).

VIII. SUMMARY

We have analyzed the effects of line broadening and redistribution of relative peak intensities in the hyperfine excitation spectra of Na atoms due to optical pumping in the weak excitation limit, when interaction times of atoms with the laser field are long compared to the characteristic optical pumping time. The study was motivated by the lack of availability of detailed theoretical models describing such effects in partially open level systems at laser intensities below the saturation limit. A number of significant results were obtained. (i) It is shown that spectral lines can be significantly broadened at laser intensities well below the saturation intensity, which is usually regarded as a threshold for onset of broadening effects. (ii) It is shown that the presence of dark m_F sublevels can vary the effective branching coefficients of the transitions, and this variation depends on laser intensity. Changes in the effective branching coefficients lead to irregular changes of peak ratios. For example, the minimum in the intensity dependence of the peak ratio deviates from the ratio expected from the given original branching coefficients. (iii) Analytical expressions are derived, which allow for the calculation of critical values for the laser intensity and Rabi frequency, above which linewidths and peak ratios are notably affected by optical pumping. (iv) It is shown that the critical laser intensity and critical Rabi frequency depend on the branching coefficient Π of the transition and that they have a minimum at $\Pi=1/2$.

Accurate theoretical simulations of the density matrix equations of motion using the split propagation technique yielded a good agreement with the experimental observations. In this study we have explored the limiting case of long interaction times of atoms with a laser field, which justified the use of the adiabatic elimination approach. It is possible, however, to obtain explicit formulas for the excitation spectra in the weak excitation limit also without the limitation of adiabaticity in switching Gaussian laser pulses. In a forthcoming publication we shall discuss some unexpected effects related to transit time broadening in the other limiting case, when the transit time is much smaller than the natural lifetime.

ACKNOWLEDGMENTS

This work was supported by the EU FP6 TOK Project LAMOL (Contract No. MTKD-CT-2004-014228), NATO Grant No. EAP.RIG.981378, INTAS, Latvian Science Council, and European Social Fund. We thank Professor K. Bergmann, Professor H. Metcalf, and Professor M. Auzinsh for helpful discussions.

[1] W. Happer, Rev. Mod. Phys. **44**, 169 (1972).
[2] C. Cohen-Tannoudji, Rev. Mod. Phys. **70**, 707 (1998).
[3] H. J. Metcalf and P. van der Straten, *Laser Cooling and Trapping* (Springer-Verlag, New York, 1999).
[4] K. Bergmann, U. Hefter, and J. Witt, J. Chem. Phys. **72**, 4777 (1980); H. M. Keller, M. Külz, R. Setzkorn, G. Z. He, K. Bergmann, and H. G. Rubahn, *ibid.* **96**, 8819 (1992).
[5] M. Auzinsh and R. Ferber, *Optical Polarization of Molecules* (Cambridge University Press, Cambridge, U.K., 1995).
[6] W. Demtröder, *Laser Spectroscopy* (Springer, Berlin, 2003).
[7] V. V. Ivanov, *Transfer of Radiation in Spectral Lines*, NBS Special Publication No. 385 (U.S. GPO, Washington, D.C., 1973).
[8] N. N. Bezuglov, A. Ekers, O. Kaufmann, K. Bergmann, F. Fuso, and M. Allegrini, J. Chem. Phys. **119**, 7094 (2003).
[9] R. M. Jopson, R. R. Freeman, W. E. Cooke, and J. Bokor, Phys. Rev. A **29**, 3154 (1984); A. Nussenzweig, E. E. Eyler, T. Bergeman, and E. Pollack, *ibid.* **41**, 4944 (1990).
[10] R. C. Ekey and E. F. McCormack, J. Phys. B **38**, 1029 (2005).
[11] C. Cohen-Tannoudji, G. Grynberg, and J. Dupont-Roc, *Atom-Photon Interactions: Basic Processes and Applications* (Wiley, New York, 1998).
[12] R. Garcia-Fernandez, A. Ekers, J. Klavins, L. P. Yatsenko, N. B. Nikolai, B. W. Shore, and K. Bergmann, Phys. Rev. A **71**, 023401 (2005).
[13] K. M. Jones, P. S. Julienne, P. D. Lett, W. D. Phillips, E. Tiesinga, and C. J. Williams, Europhys. Lett. **35**, 85 (1996).
[14] I. I. Sobel'man, *Atomic Spectra and Radiative Transitions* (Springer, Berlin, 1999).
[15] S. Stenholm, *Foundations of Laser Spectroscopy* (Wiley, New York, 1984).
[16] J. Dalibard and C. Cohen-Tannoudji, J. Opt. Soc. Am. B **2**, 1707 (1985).
[17] N. N. Bezuglov, M. Zakharov, A. N. Klyacharev A. Ekers, A. A. Matveev, K. Miculis, E. Saks, I. Sydoryk, and A. Ekers, Opt. Spectrosc. **102**, 819 (2007) [Opt. Spektrosk. **102**, 893 (2007)].
[18] N. N. Bezuglov, I. I. Beterov, A. Ekers, K. Miculis, E. Saks, A. Janovs, P. Spels, I. Sydoryk, and M. Yu. Zaharov (unpublished).
[19] N. F. Ramsey, *Molecular Beams* (Clarendon, Oxford, 1989).
[20] B. W. Shore, *The Theory of Coherent Atomic Excitation* (Wiley, New York, 1990).
[21] M. D. Feit, J. A. Fleck, and A. Steiger, J. Comput. Phys. **47**, 412 (1982).
[22] A. K. Kazansky, N. N. Bezuglov, A. F. Molisch, F. Fuso, and M. Allegrini, Phys. Rev. A **64**, 022719 (2001).